Supporting Information

Photocycle-dependent conformational changes in the proteorhodopsin cross-protomer Asp-His-Trp triad revealed by DNP-enhanced MAS-NMR

Jakob Maciejko, Jagdeep Kaur, Johanna Becker-Baldus and Clemens Glaubitz*

Institute for Biophysical Chemistry & Centre for Biomolecular Magnetic Resonance

Goethe-University Frankfurt, Germany

(*) Corresponding author.

Email: glaubitz@em.uni-frankfurt.de

Institute of Biophysical Chemistry

Goethe University Frankfurt

Max-von-Laue-Str. 9

60438 Frankfurt am Main

Germany

Tel.: +49-69-798-29927

Fax.: +49-69-798-29929

www.pnas.org/cgi/doi/10.1073/pnas.1817665116

Material & Methods

Sample preparation

The GPR gene (eBAC31A08) was cloned into a pET26b(+) vector with an adjacent TEV-protease cleavage site and 6x-His-Tag for purification. All mutations were introduced by PCR amplification of the vector with mutagenic primers and correct sequences were verified at Eurofins MWG Operon. Expression and purification of GPR_{WT} and GPR mutants was carried out as described before (1, 2). Labeled amino acids (histidine and lysine) or amino acid precursors (indole, for tryptophan labeling) were added to growing *E. coli* C43(DE3) cells once they reached an OD_{600} of 0.4. After purification and elution of the protein from Ni-NTA, the high imidazole concentration was removed by buffer exchange to TEV-cleavage buffer (150 mM NaCl, 50 mM Tris pH 8, 1 mM β-mercaptoethanol and 0.5 mM EDTA) with a PD-10 desalting column (GE Healthcare). For TEV-cleavage, TEV-protease was added to the GPR solution in a 1:5 (w/w) ratio and incubated overnight at room temperature under mild shaking. The next day TEV-protease was removed by Ni-NTA binding for 1 h at room temperature, and cleaved GPR without a 6x-His-Tag was eluted from the column. Biochemical analysis of the protein was conducted via SDS-PAGE, BN-PAGE, pH-titrations and Western-Blot (α-6x-His-Tag-alkaline phosphatase conjugated antibody (ABCAM)) as described by us before (2). GPR was reconstituted in 1,2-dimyristoyl-sn-glycero-3-phosphocholine (DMPC):1,2-dimyristoyl-sn-glycero-3-phosphate (DMPA) (9:1) proteoliposomes in a 1:2 protein to lipid (w/w) ratio using Bio-beads, according to the manufacturers instruction. Reconstitution and preparation of mixed-labeled GPR complexes was done as described before (2).

Light induced proton transport was probed on live C43(DE3) *E. coli* cells with heterologously expressed wild-type GPR or GPR mutants as described before (3-5). After expression, cells were washed several times and transferred into Pumping Buffer (10 mM NaCl, 10 mM $MgCl_2$, 1 mM $CaCl_2$). The OD_{600} was set to 16. 1 ml of the cell suspension was used for proton transport measurements. The cell suspension was subjected to an illumination protocol, consisting of 1 min in the dark, 520 nm illumination for 4 min and 2 min in the dark, during which the pH was constantly measured every 4 s under mild stirring.

DNP-enhanced solid-state NMR

For DNP-enhancement, reconstituted GPR samples were doped with AMUPol (6). Proteoliposome pellets were covered with 20 mM AMUPol solution (60% D2O, 30% glycerol-d8, 10% H2O) and were incubated overnight at 4 °C. Subsequently, the solution was completely removed and 1.5-2 mg of protein was packed into a 3.2 mm sapphire rotor. The sample was spread evenly in the MAS rotor by spinning the rotor at room temperature using a Bruker rotor testing device. Illumination procedures of the sample were executed as described before (7, 8). A high-power LED light (Mightex) with different wavelength filters was used for illumination. K-state trapping was achieved by illumination of the sample at 100 K for ~40 min with a LED power output of 3.3 W at 470 nm. M-state trapping of the GPR_{E108Q} mutant was achieved by illumination at room temperature for 90 s and subsequent freezing in liquid nitrogen. The LED power output for M-state trapping was 0.13 W at 525 nm.

DNP-enhancement solid-state NMR experiments were performed on a Bruker 400 MHz DNP system (400 MHz WB Avance II NMR spectrometer, 263 GHz Gyrotron as microwave source and 3.2 mm HCN LT-MAS probe). All spectra were recorded at 100 K and 8 kHz MAS and microwave power was set to 10.5 W. Referencing for ^{13}C and ^{15}N was done indirectly to DSS using the ^{13}C-CO signal of alanine at 179.85 ppm. For all experiments, 100 kHz decoupling using SPINAL-64 was applied during acquisition. ^{15}N-CP spectra were recorded with a CP-contact time of 800 µs and 8192 scans. ^{13}C-double quantum filter (1D-DQF) experiments were obtained with 4096 scans using the POST-C7 sequence for double quantum excitation and reconversion at 0.5 ms. 2D double quantum single

quantum (2D-DQSQ) spectra were recorded with 384 scans and 81 increments with a 17.86 µs dwell time. ^{15}N-^{15}N-PDSD spectra (9) were recorded with a mixing time of 1 s, 672 scans in the direct dimension and 110 increments in the indirect dimension with a dwell time of 125 µs. 2D-TEDOR experiments were recorded as described before (2), using a mixing time of 10.25 ms (40 rotor cycles), 1024 scans (4928 scans for GPR_{WT}-mix) in the direct dimension and 32 increments in the indirect dimension with a dwell time of 125 µs.

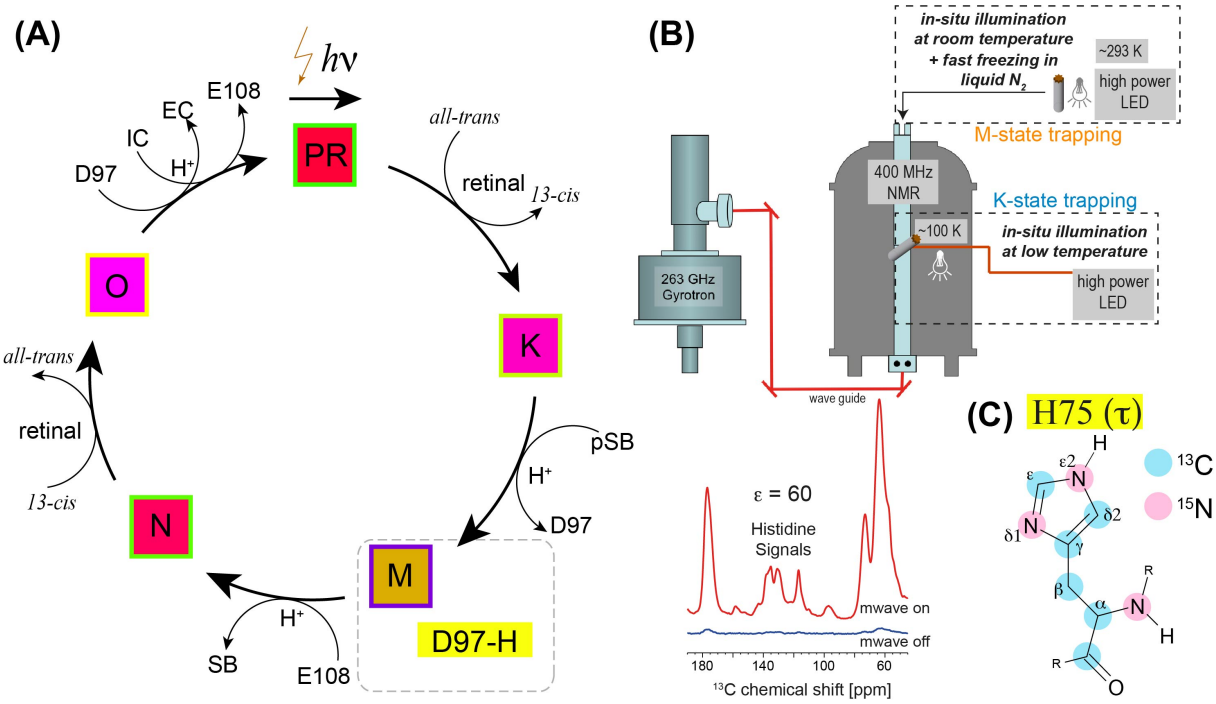

Figure S1. Procedures for trapping photocycle intermediates of GPR. (A) Photocycle of green proteorhodopsin (see text for further details). **(B)** DNP-enhanced solid-state NMR experimental setup and sample illumination procedures for K-state and M-state trapping. A 60-fold signal enhancement (ε=60) is obtained upon microwave irradiation. **(C)** Fully labeled ($^{13}C_6$, $^{15}N_3$)-H75 in the (τ)-state.

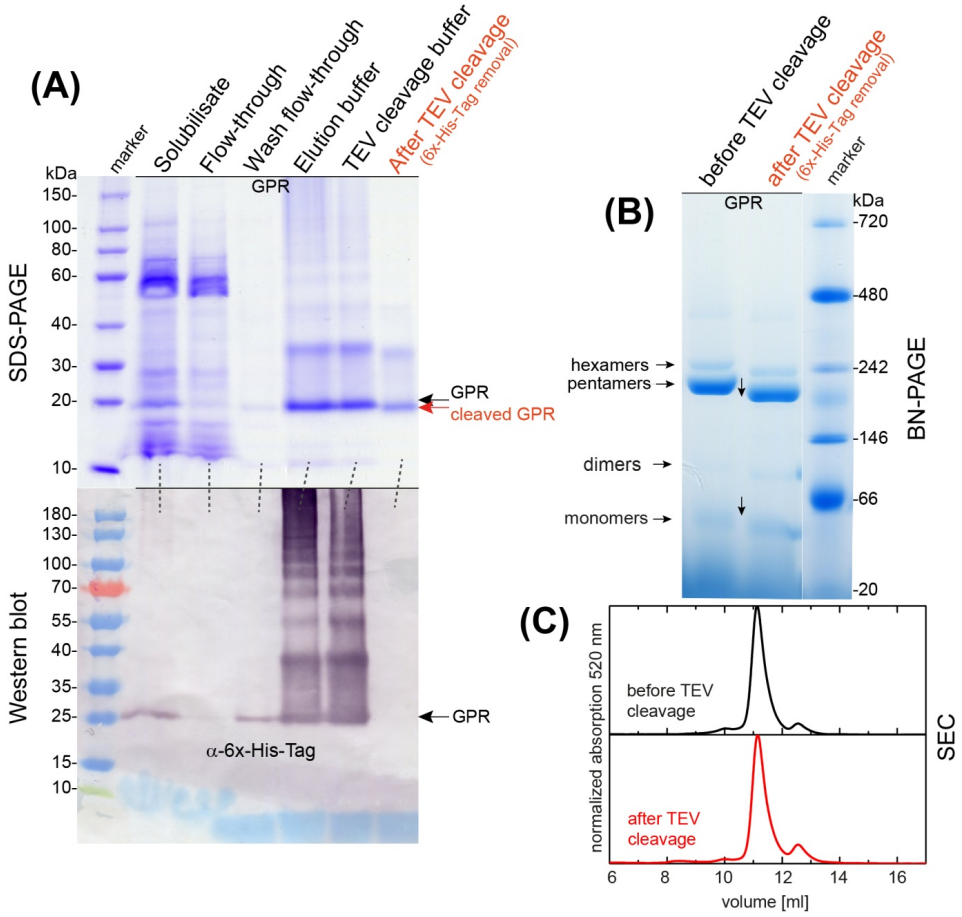

Figure S2. Purification of GPR and 6x-His-Tag removal by TEV-protease cleavage. (A) SDS-PAGE confirms the successful purification and TEV-protease cleavage of the 6x-His-Tag by a shift of the GPR band (GPR, cleaved GPR). The Western blot shows no 6x-His-Tag signal for cleaved GPR. **(B)** BN-PAGE of GPR reconstituted into proteoliposomes also shows a small shift of the protein bands but also confirms the dominant pentameric state after TEV-protease cleavage **(C)** Size exclusion chromatography (SEC) shows similar elution profiles of cleaved and non-cleaved GPR.

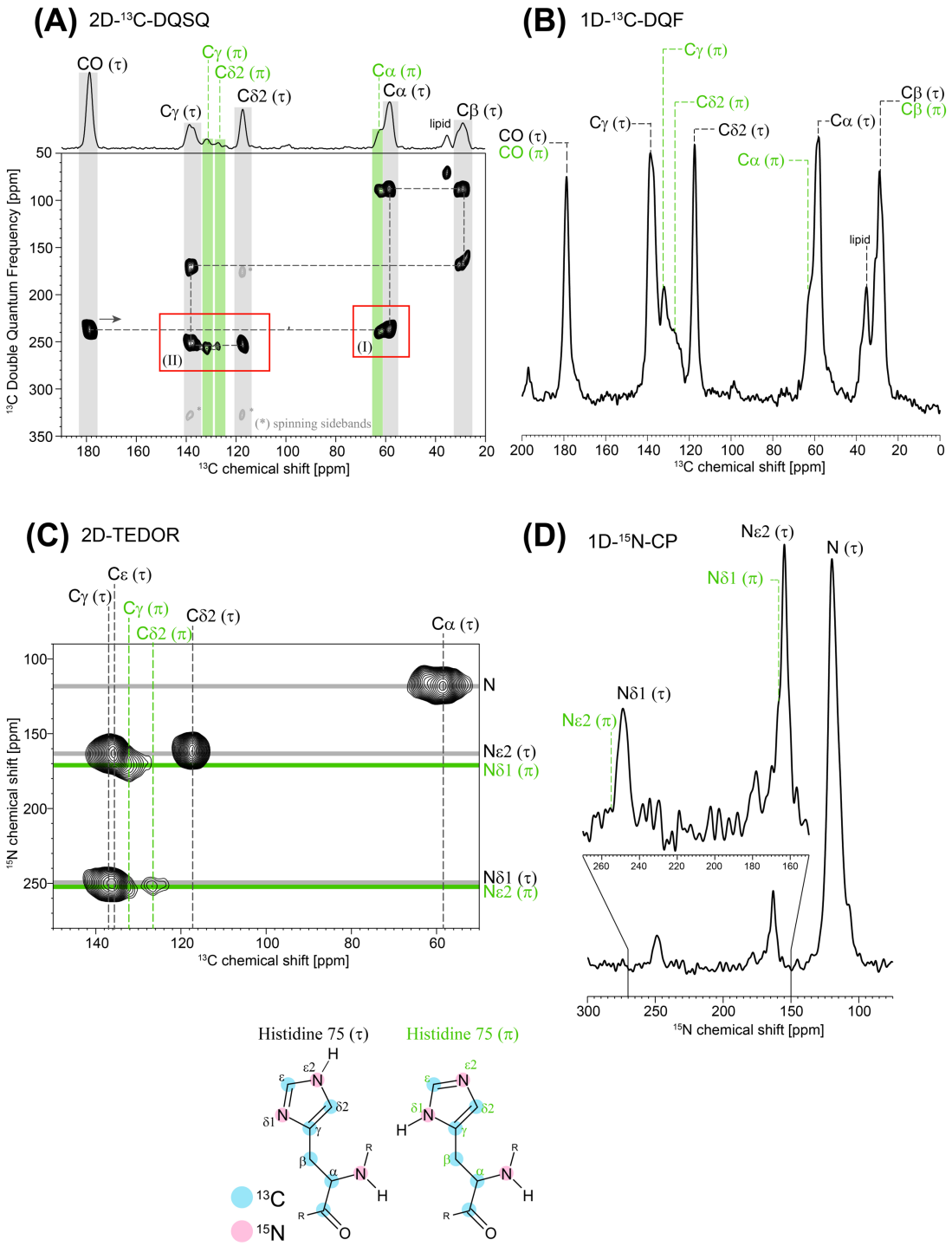

Figure S3. ^{13}C and ^{15}N chemical shift assignments of H75 in ground state ($^{13}C_6$-$^{15}N_3$-His)-GPR_{WT} (wild-type). (A) 2D ^{13}C-double quantum-single quantum (DQSQ) experiment (10). (τ)-state signals are labeled in black and (π)-state signals are labeled in green. The assignment walk through H75 in GPR_{WT} begins at the arrow and shows connectivity patterns starting from CO(τ) over Cα(τ), Cβ(τ), Cγ(τ) and finishes at Cδ2(τ). (τ)-state is the dominant state of H75 in GPR_{WT}, but also small subpopulations of (π)-state signals (green labels) can be detected for Cα (box I), Cγ and Cδ2 (box II). **(B)** The 2D-DQSQ sequential walk allows the assignment of 1D-^{13}C-double quantum filter (DQF) spectra. **(C)** 2D TEDOR spectrum (11) shows ^{13}C-^{15}N-correlations of a dominating (τ)-state and a small subpopulation of (π)-state. **(D)** ^{15}N-Cross polarization (^{15}N-CP) spectrum. Chemical shifts are summarized in Tab. S1.

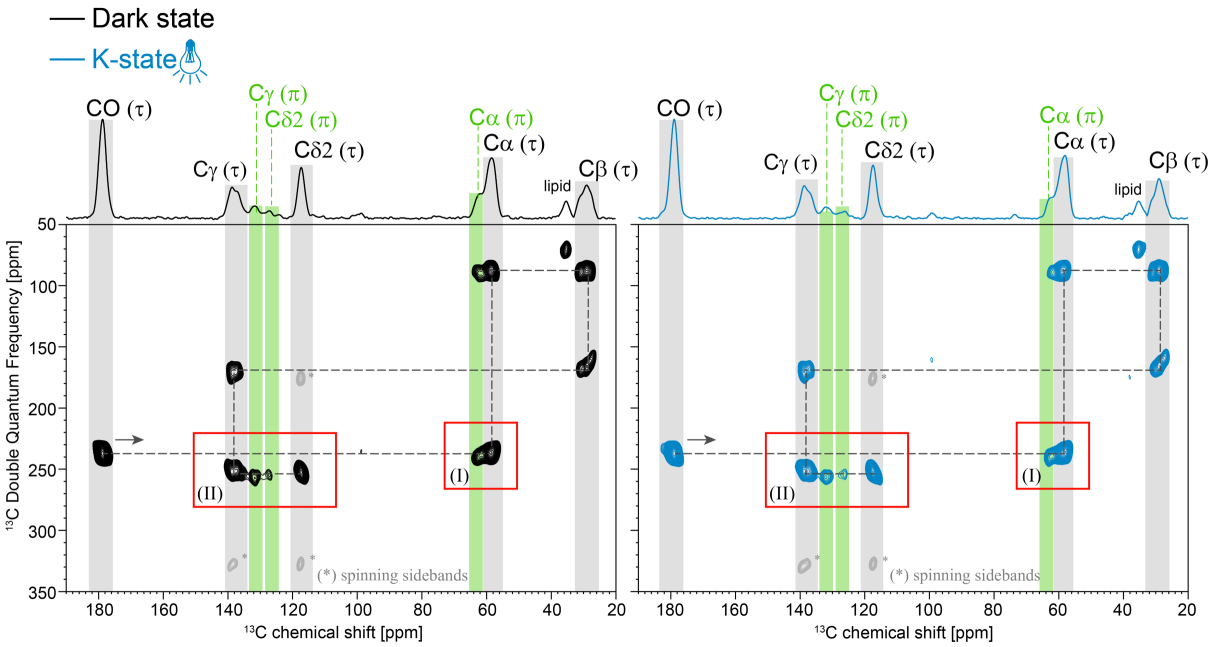

Figure S4. K-state trapping of GPR$_{WT}$. 2D ^{13}C-double quantum-single quantum (DQSQ) sequential walks of ($^{13}C_6$-$^{15}N_3$-His)-GPR$_{WT}$ in the dark state (black, left) and illuminated K-state (blue, right). No light-induced chemical shift or intensity changes can be observed for (τ)-state or (π)-state signals of Cα (I), Cγ or Cδ2 (II) in H75.

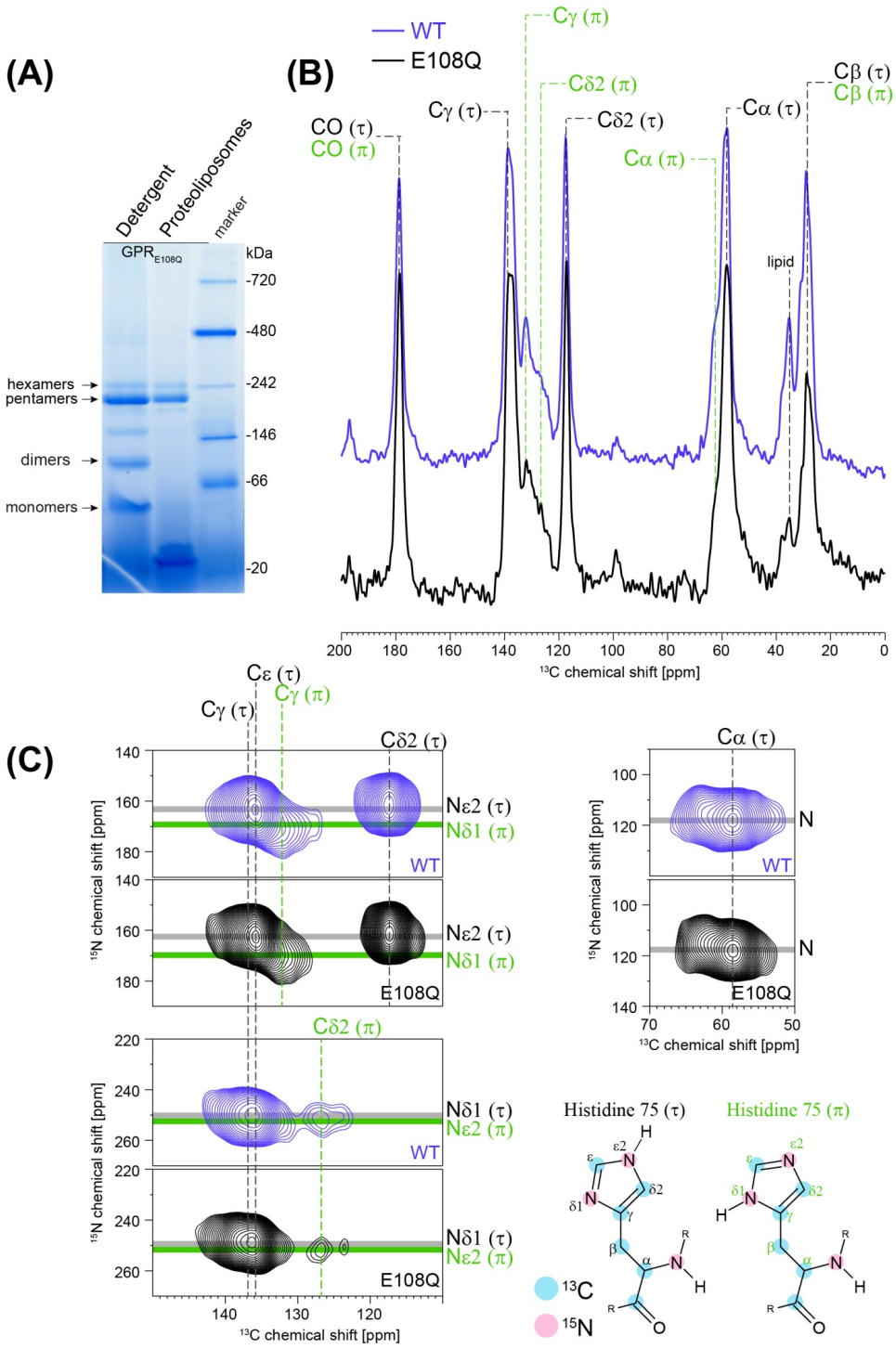

Figure S5. Comparison of GPR$_{WT}$ and the M-state trappable GPR$_{E108Q}$ mutant. (A) The M-state trappable GPR$_{E108Q}$ mutant shows a similar oligomerisation pattern as GPR$_{WT}$ in BN-PAGE. **(B)** 1D-DQF spectra of ($^{13}C_6$-$^{15}N_3$-His)-GPR$_{WT}$ (purple) and ($^{13}C_6$-$^{15}N_3$-His)-GPR$_{E108Q}$ (black) **(C)** 2D-TEDOR spectra of ($^{13}C_6$-$^{15}N_3$-His)-GPR$_{WT}$ (purple) and ($^{13}C_6$-$^{15}N_3$-His)-GPR$_{E108Q}$ (black). (τ)-state signals are labeled in black and (π)-state signals are labeled in green. The E108Q mutation does not show any structural implications for the protein or for H75 signals.

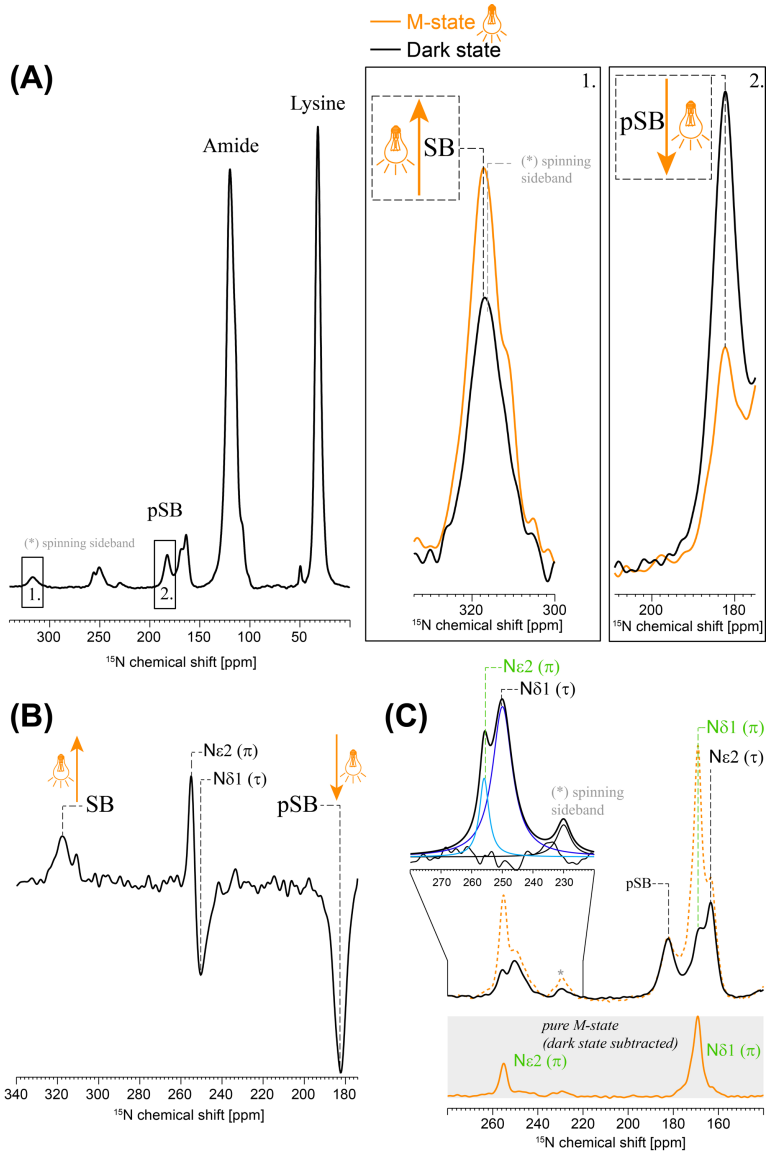

Figure S6. Deprotonation of the protonated Schiff base (pSB) during M-state trapping. (A) ^{15}N-CP spectra of ($^{13}C_6$-$^{15}N_3$-His, ^{15}Nε-Lys)-GPR$_{E108Q}$ in the dark state (black) and after illumination at RT with green light and subsequent freezing (orange). A significant reduction of the pSB signal at 182 ppm is observed. Simultaneously, the deprotonated SB signal appears at 317 ppm after illumination, confirming the specific formation of the M-state. For technical reasons, this resonance coincided with the amide spinning sideband (*). Therefore, the difference spectrum (M-state *minus* dark state) is plotted in **(B)** in order to subtract this spectral contribution from the spinning sideband. The intensity differences between SB and pSB resonances are caused by different cross-polarization efficiencies. Furthermore, a complete conversion into M-state is difficult to achieve (8), leaving a small fraction of dark state GPR after illumination as seen for the pSB resonance in (A). The changes in the H75 resonances in the M-state are explained in the main text. **(C)** As the conversion to M-state trapping after illumination is not complete, the illuminated sample contains a dark state population of the histidine. In order to determine the correct (π)/(τ)-ratio in the M-state, the dark state and M-state spectra were normalized with respect to the pSB signal. The fraction of the dark state spectrum was then subtracted from the M-state spectrum, resulting in the dark state corrected (pure M-state) spectrum, which shows almost 100% (π)-state and no presence of (τ)-state signals. In order to determine the ratio between (π) and (τ) in the dark state, the signals in the region with no other spectral overlap (around 250 ppm) were deconvoluted. The deconvoluted signals for Nε2 (π) and Nδ1 (τ) in the dark state show a ratio of approx. 1:4, which is similar to the tautomeric ratio observed for aqueous histidine.

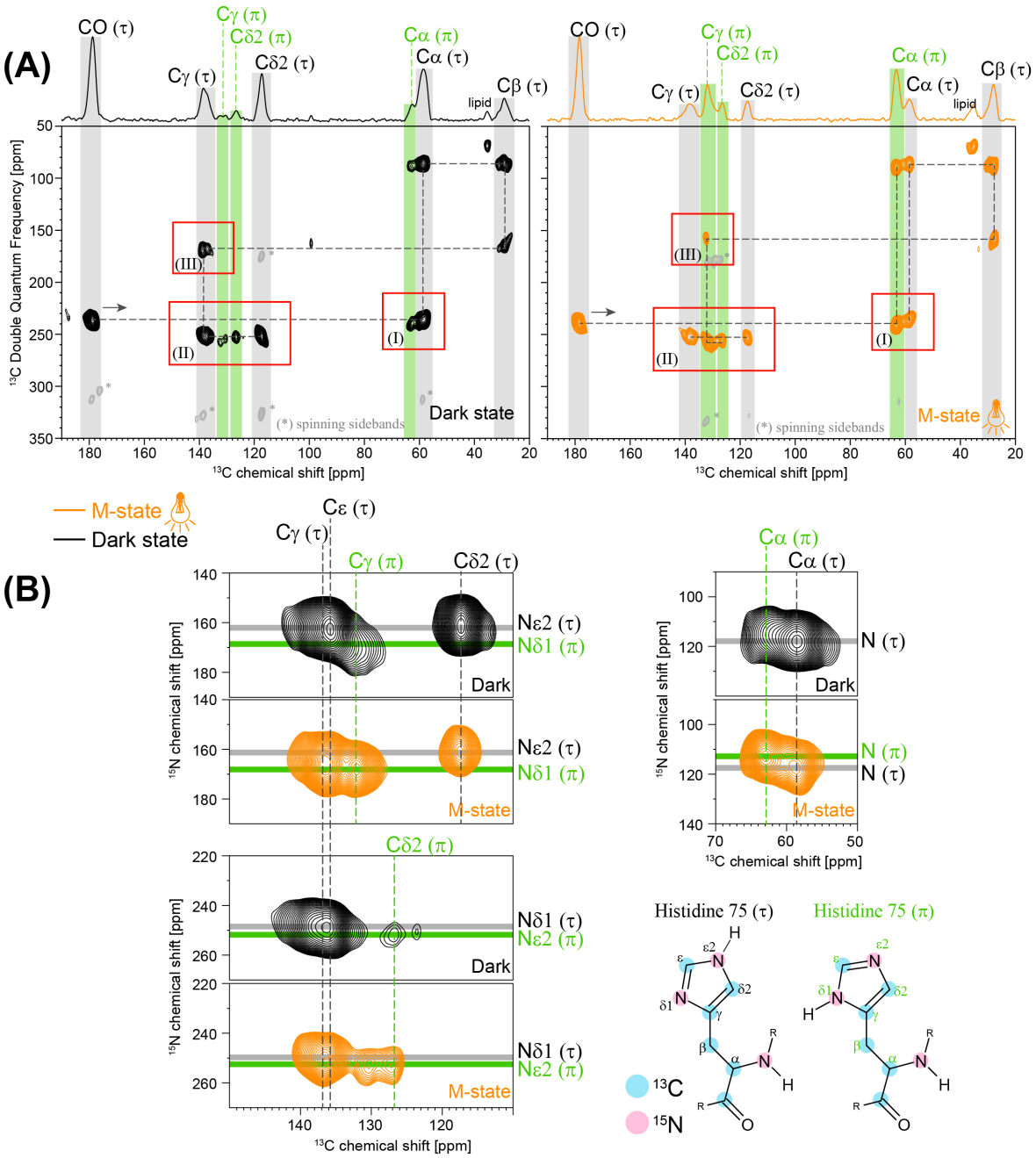

Figure S7. Effect of M-state trapping on H75 ^{15}N and ^{13}C signals in 2D-DQSQ and 2D-TEDOR spectra. (A) 2D-DQSQ spectra of ($^{13}C_6$-$^{15}N_3$-His)-GPR$_{E108Q}$ in the dark state (black) and illuminated M-state (orange). (τ)-state signals are labeled in black and (π)-state signals are labeled in green. The assignment walk through H75 in dark state begins at the arrow and shows connectivity patterns starting from CO(τ) over Cα(τ), Cβ(τ), Cγ(τ) and finishes at Cδ2(τ) (black labels). In the dark 2D-DQSQ spectrum also small subpopulations of (π)-state signals (green labels) can be detected for Cα (box I), Cγ and Cδ2 (II). The illuminated 2D-DQSQ spectrum shows increased signals for Cα (π) (I), Cγ (π) and Cδ2 (π) (II). Box III in the illuminated spectrum confirms that the imidazole ring (π)-state signal at 131.8 ppm indeed belongs to Cγ (π), as it shows direct connectivity to Cβ. Therefore, the other (π)-state signal at 131.8 ppm arising after illumination in box II must belong to Cδ2 (π). **(B)** 2D-TEDOR spectra of ($^{13}C_6$-$^{15}N_3$-His)-GPR$_{E108Q}$ in the dark state (black) and M-state (orange) also show a drastic increase of (π)-state subpopulation after illumination.

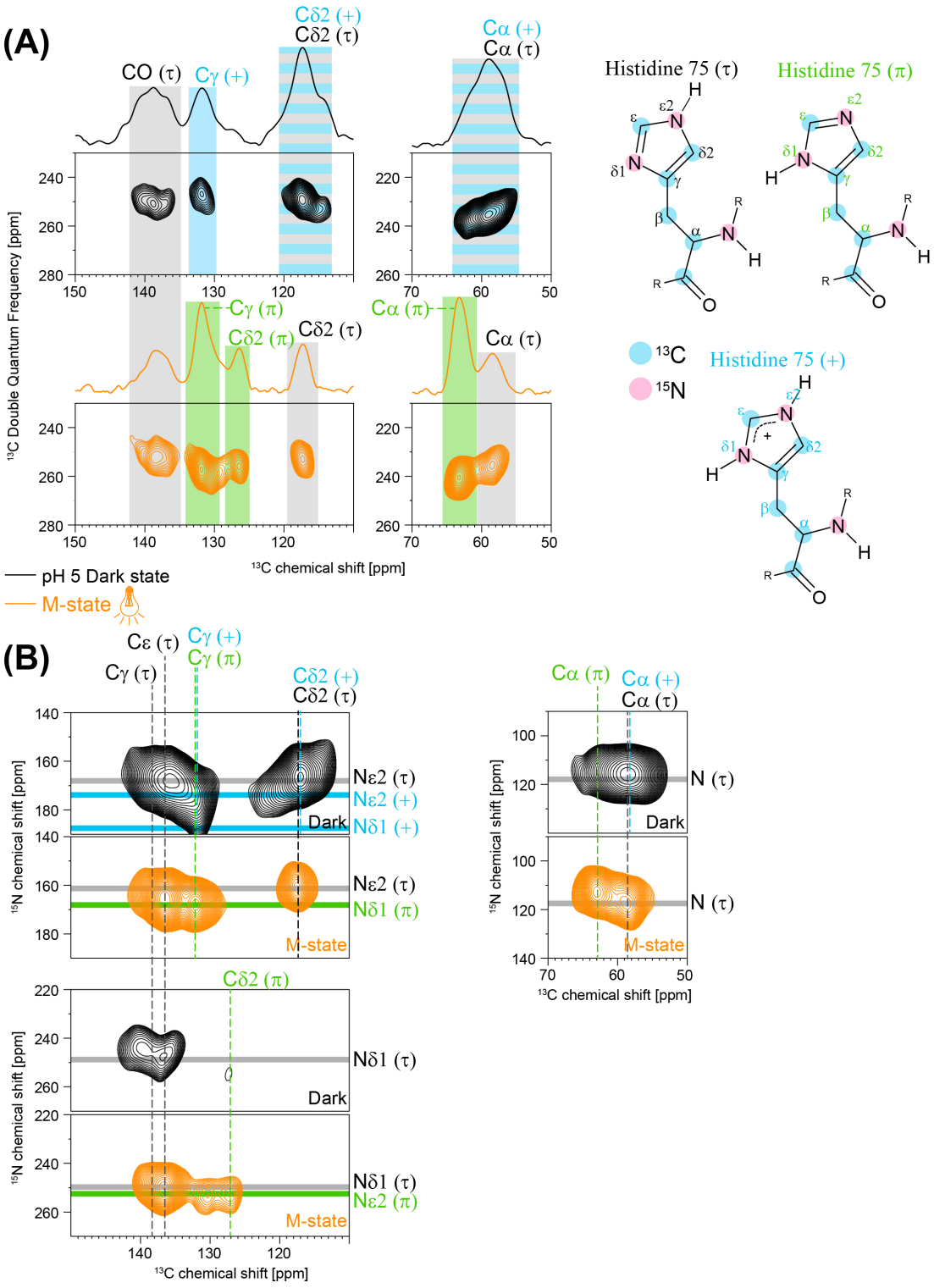

Figure S8. Comparison of GPR$_{WT}$ at pH 5 and M-state trapped GPR$_{E108Q}$. (A) 2D-DQSQ spectra of ($^{13}C_6$-$^{15}N_3$-His)-GPR$_{WT}$ in the ground state at pH 5 (black) and ($^{13}C_6$-$^{15}N_3$-His)-GPR$_{E108Q}$ in the illuminated M-state (orange). (τ)-state signals are labeled in black and (π)-state signals are labeled in green. **(B)** 2D-TEDOR spectra of ($^{13}C_6$-$^{15}N_3$-His)-GPR$_{WT}$ dark state at pH 5 (black) and ($^{13}C_6$-$^{15}N_3$-His)-GPR$_{E108Q}$ in the illuminated M-state (orange). The dark state spectrum at pH 5 corresponds to the (+)-state of H75 and shows a different signal pattern as compared to the M-state. This excludes signal contributions from the (+)-state in the M-state.

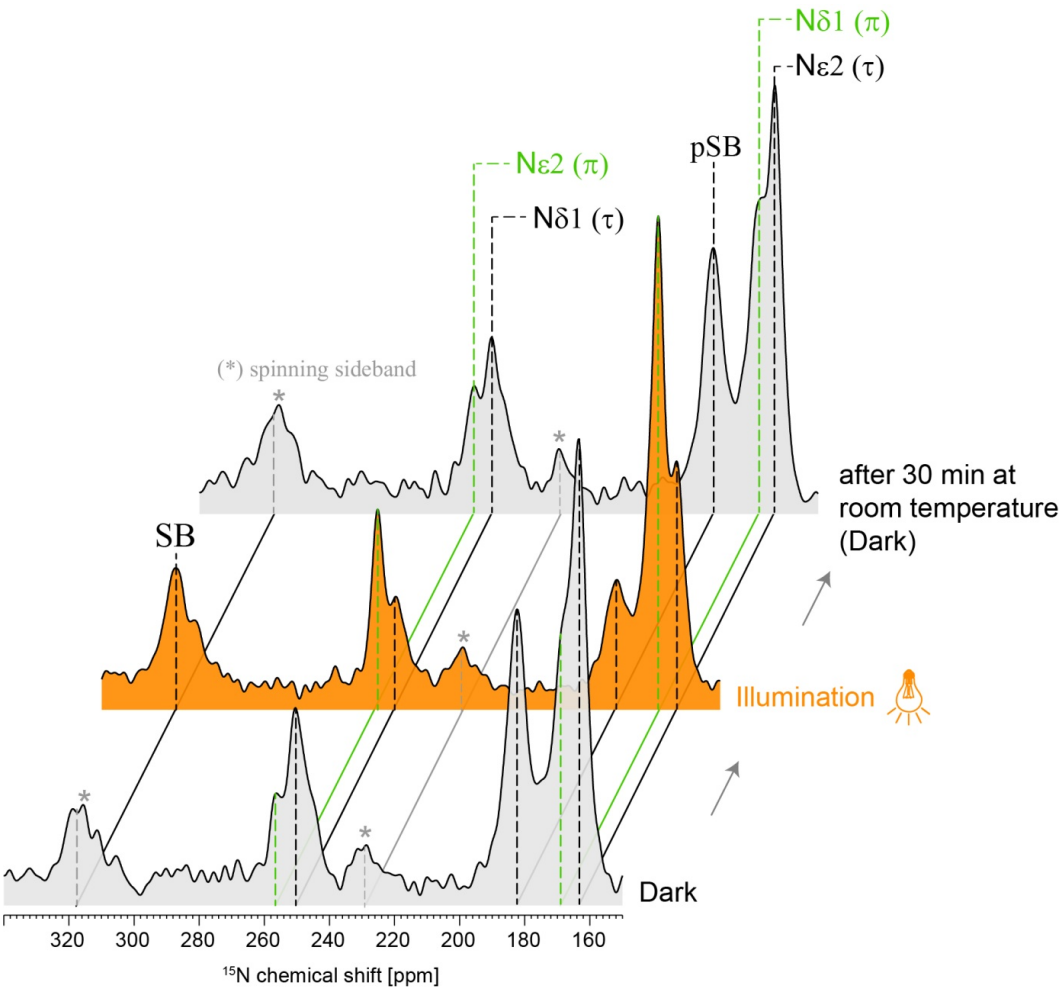

Figure S9. Reversibility of (τ) to (π) conversion during the photocycle. ^{15}N-CP spectra of ($^{13}C_6$-$^{15}N_3$-His, ^{15}Nε-Lys)-GPR$_{E108Q}$ before illumination (dark), after illumination and after thawing and incubating for 30 min at room temperature show the reversibility of M-state trapping. (τ)-state signals are labeled in black and (π)-state signals are labeled in green. After 30 min relaxation of the GPR$_{E108Q}$ sample at room temperature in the dark, the (τ)-state with protonated Nε2 and deprotonated Nδ1 reoccurs to be the dominant H75 state. This shows that the tautomerization effect is reversible and directly linked to the formation of the M-state.

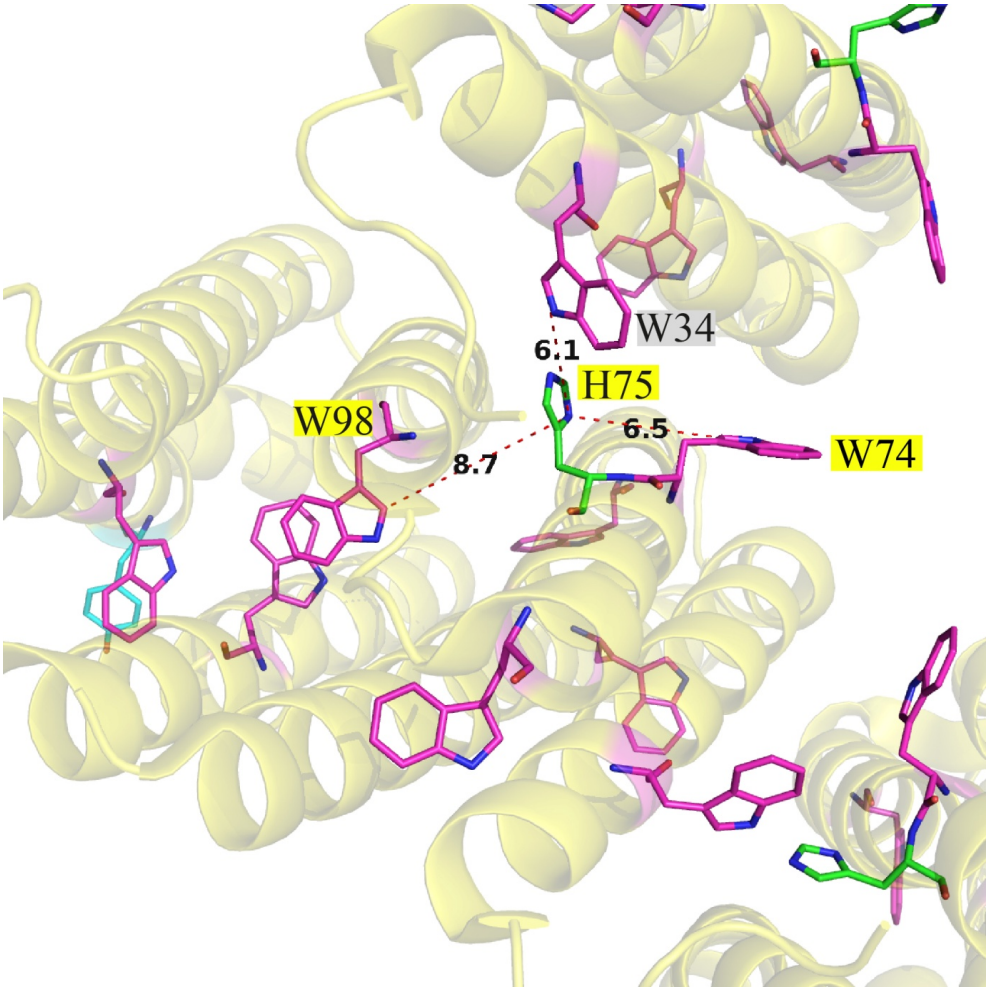

Figure S10. Distances between H75 and adjacent tryptophan residues in homologous BPR. The closest tryptophan residues to H75 are W34 across the protomer interface (6.1 Å) and neighbouring W74 (6.5 Å) (distances between W Cδ1 and H75 Nδ1). All other tryptophan residues are further than 8.7 Å (W98) away from H75 (image generated form PDB: 4KLY).

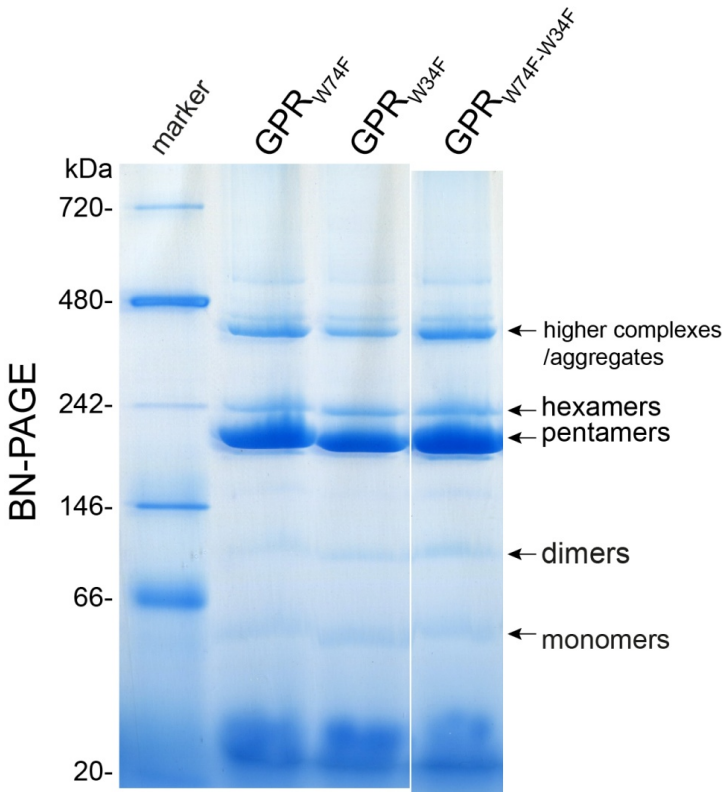

Figure S11. BN-PAGE of GPR W74 and W34 mutants, reconstituted in proteoliposomes. The single and double mutations (GPR_{W74F}, GPR_{W34F}, and $GPR_{W74F-W34F}$) do not affect the oligomeric state of the protein and show a similar oligomerisation pattern as GPR_{WT}, with a dominant pentameric form (see Figure S2).

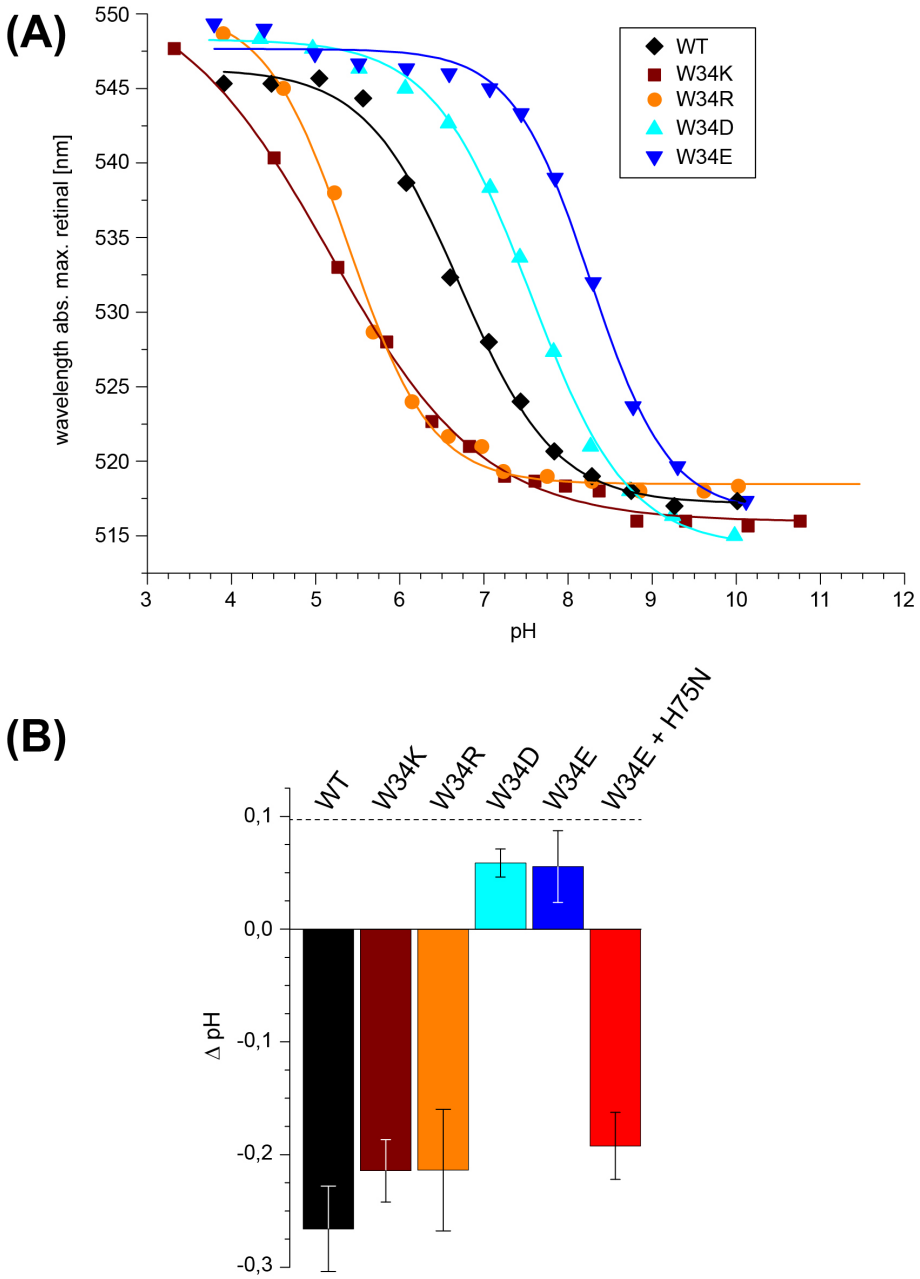

Figure S12. Effects of different W34 mutations on GPR properties. (A) pH-titrations of positively and negatively charged GPR W34 mutants. Compared to GPR_{WT} (black), positive mutations show a lower D97 pK_a value and negative mutations show a higher D97 pK_a value. The measurements were carried out on PR solubilized in DDM as described previously (2). **(B)** Whole cell proton transport measurements in live *E. coli* cells containing heterologously expressed W34 mutants. The cell suspension was subjected to 520 nm illumination for two minutes, during which the pH was constantly monitored (3-5). GPR_{WT} shows a pH decrease upon illumination, corresponding to outward driven proton transport. Positive mutations (GPR_{W34K} and GPR_{W34R}) do not show a drastic effect on proton transport. Negative mutations (GPR_{W34D} and GPR_{W34E}) exhibit a reverse proton transport, indicated by pH increase. The double mutation of $GPR_{W34E\text{-}H75N}$ again reverses the effect and shows normal outward proton transport. This indicates that the effect on the functional residue D97 from the W34E mutation is mediated by H75.

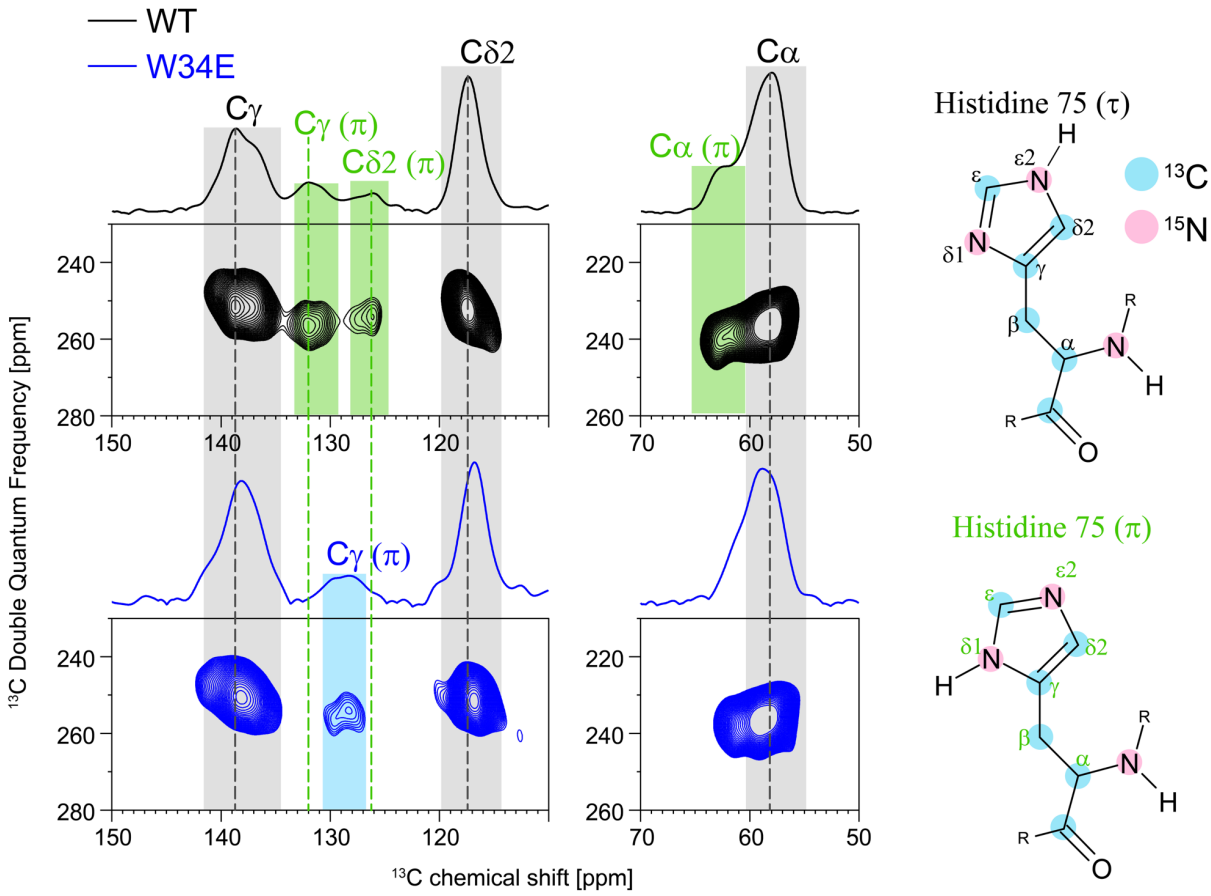

Figure S13. Comparison of GPR_{WT} and GPR_{W34E} H75 signals. 2D-DQSQ spectra are shown of ($^{13}C_6$-$^{15}N_3$-His)-GPR_{WT} (black) and ($^{13}C_6$-$^{15}N_3$-His)-GPR_{W34E} (blue) at pH9 ((τ)-state black, (π)-state green). For GPR_{WT} the small (π)-state subpopulation is detectable for Cγ, Cδ2 and Cα. In the W34E mutant Cγ(π) is shifted by 4 ppm (129 ppm) and Cδ2(π) merges with the dominant Cδ2(τ) signal. The chemical shift changes could reflect alterations of the H75 structure and orientation in GPR_{W34E}, which might cause the drastic pK_a shift of D97 and reverse proton transport.

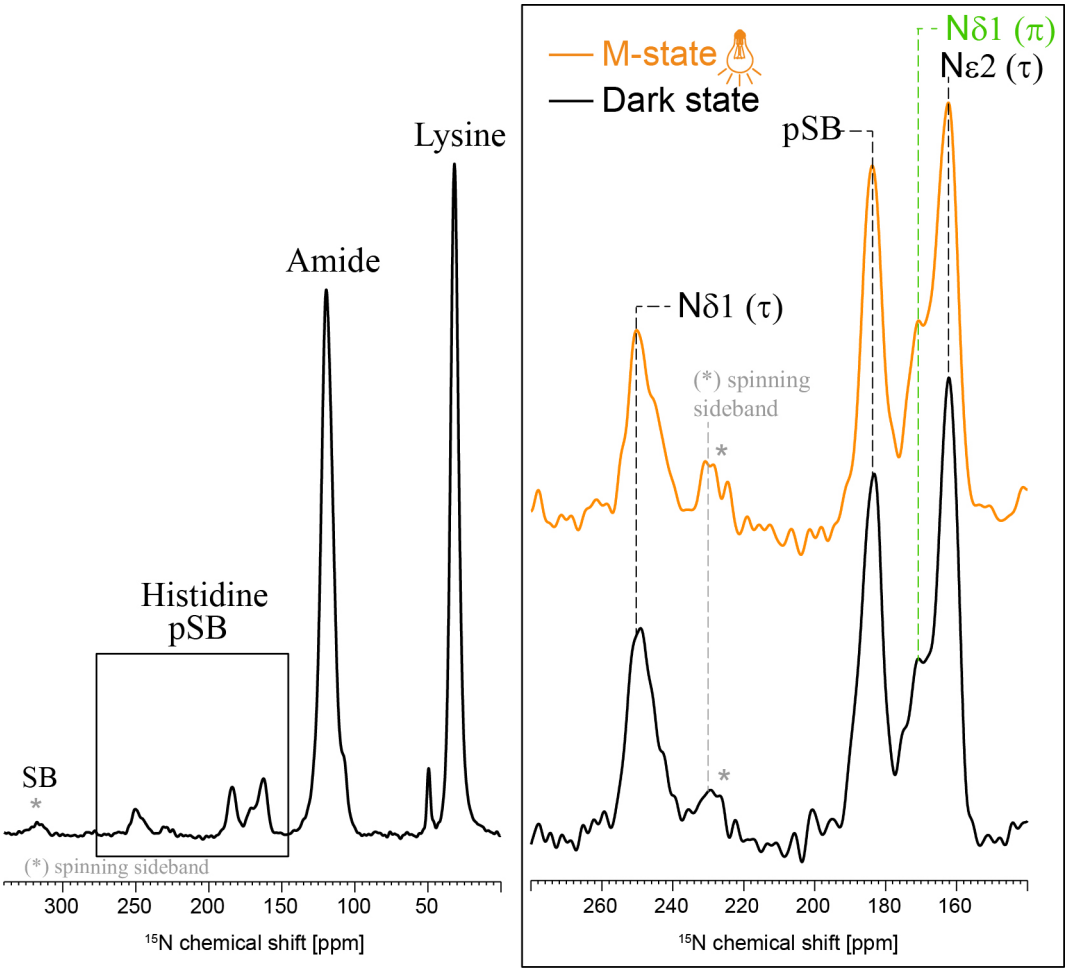

Figure S14. Illumination of the double mutant GPR$_{E108Q-W34E}$. ^{15}N-CP spectra are displayed of (^{13}C$_{\square}$-^{15}N$_3$-His, ^{15}Nε-Lys)-GPR$_{E108Q-W34E}$ in the dark state (black) and M-state (orange) ((τ)-state black, (π)-state green). No changes in the pSB, SB or the tautomeric state of H75 can be detected.

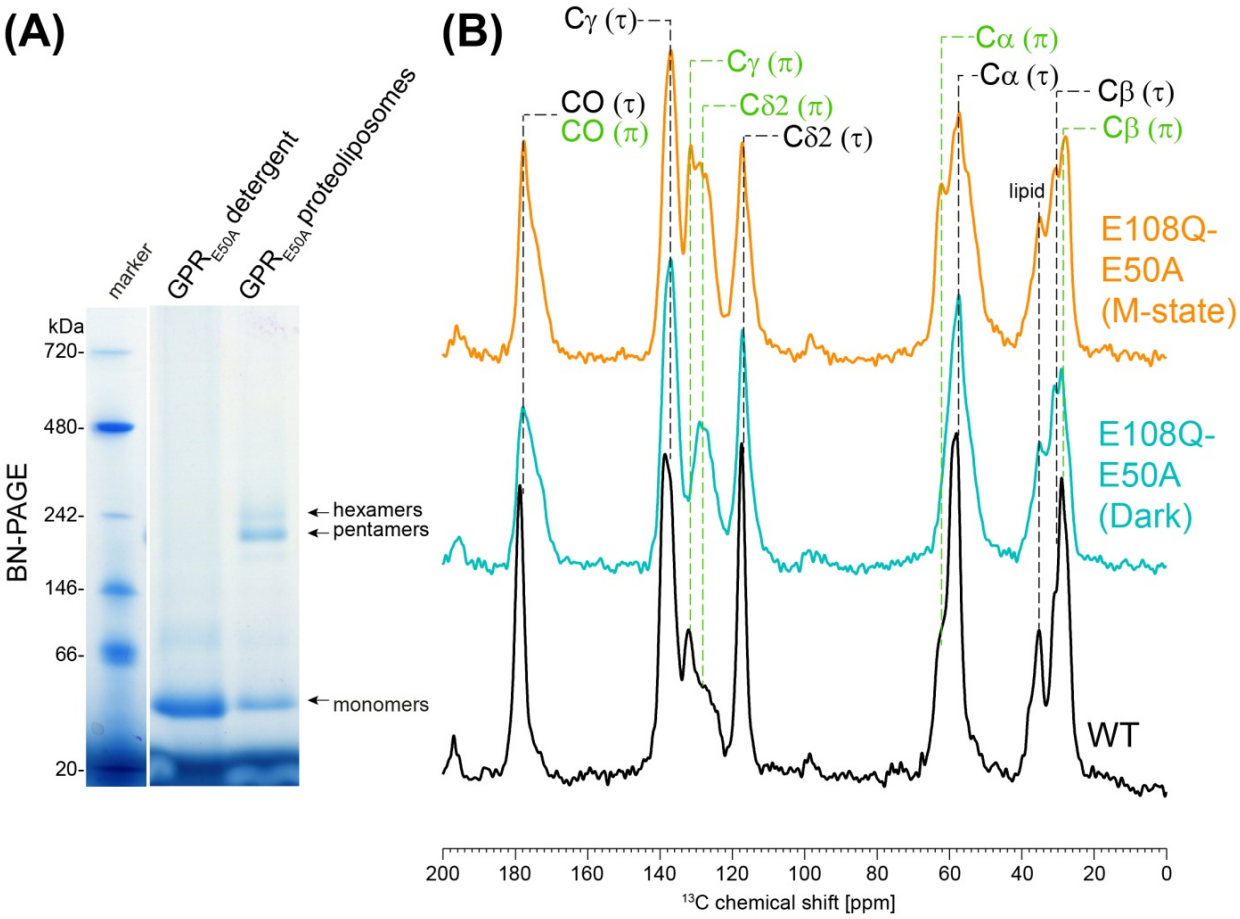

Figure S15. Effect of oligomer disruption on H75 signals. (A) BN-PAGE of GPR$_{E50A}$ in detergent (0.05% DDM) and reconstituted in proteoliposomes. The E50A mutation causes a disruption of higher oligomeric complexes in detergent, where monomers constitute the dominant form. After reconstitution, a higher amount of monomeric protein remains compared to GPR$_{WT}$ (Fig. S2), showing that the mutation has a destabilizing effect on the complex. **(B)** 1D-DQF spectra of ($^{13}C_6$-$^{15}N_3$-His)-GPR$_{WT}$ (black), ($^{13}C_6$-$^{15}N_3$-His)-GPR$_{E108Q-E50A}$ in the dark state (light blue) and ($^{13}C_6$-$^{15}N_3$-His)-GPR$_{E108Q-E50A}$ in the illuminated M-state (orange). (τ)-state signals are labelled in black and (π)-state signals are labelled in green. Compared to GPR$_{WT}$, the disrupting effect of E50A mutation causes peak broadening for ^{13}C histidine signals, indicating more possible orientations and a higher flexibility of the residue. The H75 tautomerization efficiency is much less for GPR$_{E108Q-E50A}$, indicating that a stable cross-protomer contact to W34 is needed to force H75 into the new tautomeric form.

Table S1: (τ) and (π)-states chemical shifts (CS) of H75. The chemical shifts were detected in ^{13}C-2D-DQSQ, ^{13}C-DQF, 2D-TEDOR and ^{15}N-CP spectra (Fig. S6).

Site	(τ) CS [ppm]	(π) CS [ppm]
N	119.2	114.1
Nδ1	250.4	169.1
Nε2	163.5	255.2
CO	178.6	177.8
Cα	58.2	63.0
Cβ	28.8	27.5
Cγ	137.7	131.8
Cδ2	117.2	126.6

References

1. Mehler M, *et al.* (2013) The EF loop in green proteorhodopsin affects conformation and photocycle dynamics. *Biophys. J.* 105(2):385-397.
2. Maciejko J, *et al.* (2015) Visualizing Specific Cross-Protomer Interactions in the Homo-Oligomeric Membrane Protein Proteorhodopsin by Dynamic-Nuclear-Polarization-Enhanced Solid-State NMR. *J. Am. Chem. Soc.* 137(28):9032-9043.
3. Maresca JA, Keffer JL, & Miller KJ (2016) Biochemical Analysis of Microbial Rhodopsins. *Current protocols in microbiology* 41:1F 4 1-1F 4 18.
4. Ganapathy S, *et al.* (2015) Modulation of spectral properties and pump activity of proteorhodopsins by retinal analogues. *Biochem. J.* 467(2):333-343.
5. Ganapathy S, *et al.* (2017) Retinal-Based Proton Pumping in the Near Infrared. *J. Am. Chem. Soc.* 139(6):2338-2344.
6. Sauvee C, *et al.* (2013) Highly efficient, water-soluble polarizing agents for dynamic nuclear polarization at high frequency. *Angew. Chem. Int. Ed. Engl.* 52(41):10858-10861.
7. Becker-Baldus J, *et al.* (2015) Enlightening the photoactive site of channelrhodopsin-2 by DNP-enhanced solid-state NMR spectroscopy. *Proc Natl Acad Sci U S A* 112(32):9896-9901.
8. Mehler M, *et al.* (2017) Chromophore Distortions in Photointermediates of Proteorhodopsin Visualized by Dynamic Nuclear Polarization-Enhanced Solid-State NMR. *J. Am. Chem. Soc.* 139(45):16143-16153.
9. Szeverenyi NM, Sullivan MJ, & Maciel GE (1982) Observation of spin exchange by two-dimensional fourier-transform C-13 cross polarization-magic-angle spinning. *J. Magn. Reson.* 47(3):462-475.
10. Hong M (1999) Solid-state dipolar INADEQUATE NMR spectroscopy with a large double-quantum spectral width. *J. Magn. Reson.* 136(1):86-91.
11. Jaroniec CP, Filip C, & Griffin RG (2002) 3D TEDOR NMR experiments for the simultaneous measurement of multiple carbon-nitrogen distances in uniformly (13)C,(15)N-labeled solids. *J. Am. Chem. Soc.* 124(36):10728-10742.